Impact of flow configuration on electrosorption performance and energy consumption of CDI systems

Lutfi Agartan, Bilen Akuzum, Ertan Agar and E. Caglan Kumbur

ABSTRACT

The flow configuration selected for a capacitive deionization (CDI) system can impact the desalination performance due to drastic changes to the ion transport. Herein, a zero-gap CDI cell fixture with various flow configurations was utilized to investigate the effects of flow directionality on the CDI performance of activated carbon cloth (ACC) electrodes. Salt adsorption capacities and salt adsorption rates were determined for three commonly studied flow field designs (parallel (PFF), interdigitated (IDFF), and serpentine (SFF)) at various flow rates (2–128 mL/min). Increasing the flow rate was found to result in decreasing CDI performance for SFF and IDFF designs. On the other hand, the peak performance was observed for the parallel flow field at 32 mL/min flow rate. Additionally, the pressure drop values for different flow configurations were measured, and the energy consumptions were calculated. Overall, the findings showed that the performance of CDI systems strongly depends on the selected flow field geometry. Among the tested flow fields, the parallel configuration offered the best balance between CDI performance and energy efficiency. However, the designs that exert high hydrodynamic forces on the electrode plane showed poor performance due to rip-off of ions from the double layer causing a significant capacity loss for ACC electrodes.

Key words | capacitive deionization, electrosorption kinetics, flow configuration, salt adsorption rate, water desalination

Lutfi Agartan
Bilen Akuzum
E. Caglan Kumbur (corresponding author)
Electrochemical Energy Systems Laboratory,
Department of Mechanical Engineering and Mechanics,
Drexel University,
Philadelphia, PA 19104,
USA
E-mail: *eck32@drexel.edu*

Ertan Agar
Department of Mechanical Engineering,
University of Massachusetts Lowell,
Lowell, MA 01854,
USA

HIGHLIGHTS

- CDI performance strongly depends on the flow directionality of water.
- Energy consumption of a CDI system strongly depends on the flow directionality.
- Higher flow rates elevate the effects of flow fields on the CDI performance.
- Parallel flow field provides a lower pressure drop with higher CDI performance.
- Higher hydrodynamic forces can lead to ion rip-off from the diffuse layer.

INTRODUCTION

Capacitive deionization (CDI) is considered to be a promising technology for water desalination due to its lower energy demand and operational costs compared to traditional desalination technologies like reverse osmosis and distillation (Porada *et al.* 2013; Suss *et al.* 2015). During operation, the electrodes are polarized, while saline water is passing through the CDI cell. The applied potential forms the electric double layer (EDL) on the surfaces of the electrodes, causing ions to migrate toward the electrodes. Upon reaching the surface, ions are adsorbed and salinity of the water decreases (Porada *et al.* 2013; Suss *et al.* 2015). The polarization is either removed or reversed for releasing the ions and regenerating the electrodes for subsequent salt adsorption (Porada *et al.* 2013; Suss *et al.* 2015).

Although CDI offers an energy-efficient solution to water desalination, the salt removal performances of these systems have not yet reached a level where they are competitive with conventional desalination techniques. The salt removal

doi: 10.2166/aqua.2020.012

performances of CDI systems are shown to depend on (i) operating conditions (i.e., applied potential, flow rates, salt type, and concentration) (Gabelich Tran & Suffet 2002; Mossad & Zou 2012; Han *et al.* 2014; Aldalbahi *et al.* 2018), (ii) cell architectures (i.e., membrane CDI, flow electrode CDI, inverted CDI, and hybrid CDI) (Biesheuvel & van der Wal 2010; Jeon *et al.* 2013; Lee *et al.* 2014; Gao *et al.* 2015), and (iii) electrode materials (i.e., novel carbon materials, such as CNT and graphene, metal oxides (MnO_2), metal carbides (Ti_3C_2), and surface treatment of the electrodes) (Gabelich Tran & Suffet 2002; Ryoo *et al.* 2003; Yang *et al.* 2011; Porada *et al.* 2013; Gao *et al.* 2015; Laxman *et al.* 2015; Omosebi *et al.* 2015; Srimuk *et al.* 2016; Agartan *et al.* 2018, 2019). Although notable performance improvements are achieved with most of these approaches, the commercialization aspect of CDI systems has been overlooked. When industrial applications are considered, some of these approaches are not feasible because they require either lengthy procedure times (i.e., surface treatment of electrodes (Huang *et al.* 2014) and synthesis of new materials (Yang *et al.* 2011; Srimuk *et al.* 2016)) or expensive chemicals and materials (i.e., ion exchange membranes (Biesheuvel & van der Wal 2010; Yang *et al.* 2011; Srimuk *et al.* 2016) and novel electrodes (Yang *et al.* 2011; Lee *et al.* 2014; Srimuk *et al.* 2016)). These drawbacks make it difficult for CDI systems to be scaled up to industrial level and widespread use of it for commercial applications.

The design of robust flow cell architectures could be a cost-effective approach in improving performance in the CDI systems without altering the electrode structure. Over a dozen CDI cell designs have been reported in the literature so far, with many of them offering various advantages (Lee *et al.* 2011, 2014; Jeon *et al.* 2013; Gao *et al.* 2015; Remillard *et al.* 2018). However, to the best of the authors' knowledge, the availability of studies comparing CDI performance metrics of different CDI flow configurations has been fairly limited. On the other hand, an abundance of studies investigating the efficacy of different flow field configurations for fuel cells and redox flow batteries (RFBs) has offered great insights for the effective cell design of the respective technologies (Wang 2015; Dennison *et al.* 2016; Houser *et al.* 2017). In flow-assisted electrochemical systems, the charge transport performance of the system greatly depends on the mass transport of the active species in the cell. This effect can be clearly observed in systems such as RFBs, where the flow configurations that generate forced-flow into the electrodes (i.e., interdigitated and serpentine (Dennison *et al.* 2016; Houser *et al.* 2017)) usually result in much higher power output due to increased convection and species transport to the electrode surface. Contrary to the faradaic systems, in capacitive electrochemical systems (i.e., CDI and flow capacitor (Porada *et al.* 2013; Suss *et al.* 2015; Ratajczak *et al.* 2019)), the convective flow could have detrimental effects to the electrochemical performance due to disruption of the double layer structure by hydrodynamic forces. In this manner, it is crucially important to understand the relationship between flow directionality and electrochemical performance for the CDI systems.

In this work, we seek to investigate the influence of flow configurations (i.e., flow field and flow rate) on the salt adsorption capacity (SAC), the electrosorption kinetics, the pressure drop, and the energy consumption of a lab-scale CDI system. Specifically, the goal is to develop an understanding of the impact of flow configurations on the performance metrics of a CDI system. To accomplish this goal, 15 different cases of flow configurations have been systematically studied by changing the flow field design and the flow rate of the saline water. Commercially available activated carbon cloths (ACC) have been used as electrodes in the symmetric CDI setup. Interdigitated (IDFF), serpentine (SFF), and parallel (PFF) flow field designs and flow rates of 2, 8, 32, 64, and 128 mL/min have been employed for desalination tests. Chronoamperometry (CA) and ionic conductivity data have been gathered to gauge the effects of flow configurations on the salt removal performance of the CDI setup. Additionally, pressure drops have been recorded to gain a better understanding of the relationship between pumping losses and flow configurations. Lastly, the energy needed for charging the electrodes and pumping the saline water has been calculated to establish a correlation between the energy consumption and the selected flow configuration for the CDI system.

EXPERIMENTAL PROCEDURE

Materials

As received Zorflex FM50 K activated carbon cloth (Charcoal House LLC) and Celgard 3501 are used as the porous

carbon electrodes and the separator for the CDI tests, respectively. A laser cutter (Full Spectrum Laser H-Series 4th Generation) is employed to cut the electrodes and the separators used in the CDI tests. The electrodes employed for the CDI testing have a specific surface area of 1,355 m^2/g, a pore volume of 0.53 cm^3/g, an average pore size of 0.61 nm, a thickness of 500 μm, and a geometric area of 10 cm^2 (3.16 cm × 3.16 cm). Separators used for the tests had the dimensions of 5 cm × 5 cm.

CDI setup and flow configurations

CDI tests are conducted in batch mode using a glass vial having 50 mL of a 10 mM sodium chloride (NaCl) solution, which is circulated through the CDI cell by a peristaltic pump (Watson-Marlow 505Du). The circulated water is collected again in the same glass vial, in which the ionic conductivity probe (Mettler Toledo, InLab 731-ISM) is dipped to measure the ionic conductivity of the solution *in operando*. The ionic conductivity data gathered by the probe are transmitted to an ionic conductivity meter (Mettler Toledo, S470 SevenExcellence), where the data is recorded every 10 s using the LabX® direct software. Chronoamperometry, an electrochemical technique that applies a constant voltage, is applied by a Biologic VMP3 potentiostat to the CDI cell for cycling between 1.2 V for charging and 0 V for discharging for 10 min for each half-cycle.

A zero-gap flow cell is employed for the CDI cell setup, where the current collectors, electrodes, and separators are pressed into a sandwich structure with no space in between (see Figure 1). Water is pumped through the flow fields (i.e., IDFF, SFF, and PFF designs; see Figure 2) machined into the graphite plates. The influent water enters the cell from the inlets located at each upper side corner of the cell, and follows the flow field, to the outlets of the setup on both sides to leave the cell. The machined flow fields have the width, depth, and length of 1 mm, 1 mm, and 30 mm, respectively. Different flow fields are designed to steer the fluid in the channel in different directions and planes. The IDFF and SFF designs force the water to move in the *z*-direction (toward the electrode plane; see Figure 2(a) and 2(b)). However, water moves in the *xy*-plane in the flow channels of the PFF design due to the open-ended design of flow channels.

These flow fields are tested across a wide range of flow rates: 2, 8, 32, 64, and 128 mL/min. Each case is named using the flow field design and applied flow rate. For instance, IDFF_2 nomenclature stands for the case where an interdigitated flow field is employed, and 2 mL/min flow rate is applied. The effects of flow configuration (i.e., flow field design and flow rate) on the SAC of CDI systems are investigated by the following equation:

$$\text{SAC (mg of salt/g of electrode)} = \frac{\Delta C \times V \times \text{MW}_{\text{NaCl}}}{m} \quad (1)$$

where ΔC stands for the concentration change (M), V is the volume (L) of the saline solution, MW_{NaCl} is the molecular weight of NaCl (58.44 g/mol), and m is the total mass of the electrodes (g). Charge efficiency (Λ) is another important performance metric for the CDI systems. It is defined as the ratio of the charge equivalent of the adsorbed salt to the amount of the charge stored during the charging half

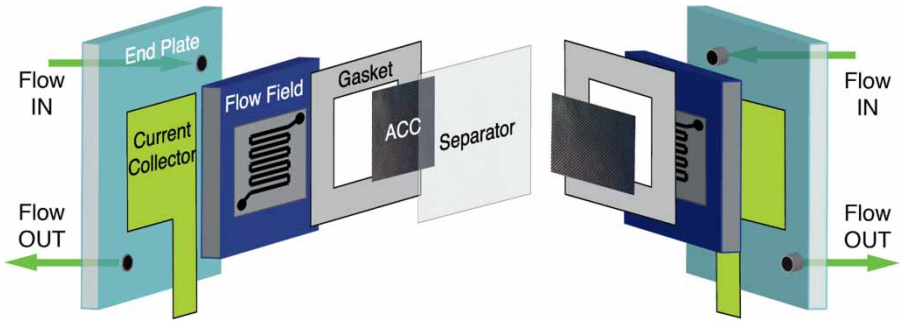

Figure 1 | CDI cell schematic.

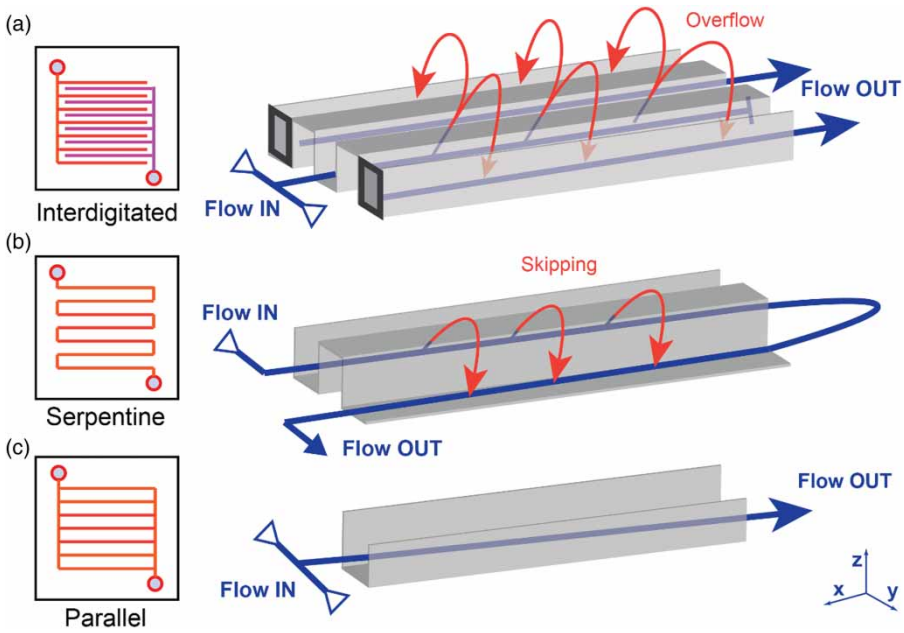

Figure 2 | Schematic of (a) IDFF, (b) SFF, and (c) PFF designs.

cycle and is calculated by the following equation:

$$\Lambda(\%) = \frac{\Delta C \times V \times \mathrm{F}}{Q_s} \times 100 \tag{2}$$

where F is the Faraday's constant (96,485 C/mol), and Q_s is the amount of charge stored (C). Alongside the SAC and the charge efficiency, electrosorption kinetics is also critical for the performance analyses of a CDI system. Electrosorption kinetics is analyzed using the *in situ* salt adsorption rate (SAR) vs SAC plots (Kim & Yoon 2015; Agartan *et al.* 2018). The graphs are prepared by plotting the salt adsorption rates (SAR (mg/g min)) with respect to the SAC (mg/g) values (Kim & Yoon 2015). SAR is calculated from the change of ion concentration by time using the following equation:

$$\mathrm{SAR\,(mg\,of\,salt/g\,of\,electrode\text{-}min)} = \frac{\Delta C \times V \times \mathrm{MW_{NaCl}}}{m \times t} \tag{3}$$

The total energy consumption of the CDI system per gram of removed salt (Wh/g of removed salt) is calculated by summing up the pumping energy (Equation (4)) and charging energy (Equation (5)) required for the removal of a gram of salt. The pumping energies are calculated using the measured pressure drop values across the cell by the following equation (Houser *et al.* 2017):

$$\mathrm{Pumping\ energy\ (Wh/g\ of\ removed\ salt)} = \frac{\Delta p \times \dot{V}}{\eta_{\mathrm{pump}} \times V \times \Delta C \times \mathrm{MW_{NaCl}}} \times t \tag{4}$$

where Δp is the pressure drop (Pa), $\dot{V}$ is the flow rate (m^3/s), η_{pump} is the pump efficiency, t is the charging half-cycle length (s). The energy needed for charging the cell for removing a gram of salt is calculated using the following equation (Mossad & Zou 2012):

$$\mathrm{Salt\ removal\ energy\ (Wh/g\ of\ removed\ salt)} = \frac{\varphi \times Q_s}{V \times \Delta C \times \mathrm{MW_{NaCl}}} \tag{5}$$

where φ is the applied potential (V).

RESULTS AND DISCUSSION

Flow configurations and their effects on the system performance is a well-established field for faradaic flow-assisted electrochemical energy systems (i.e., RFBs, fuel cells, etc.) (Dennison *et al.* 2016; Houser *et al.* 2017). The power output of RFBs can be significantly improved by selecting

flow field designs that can enhance the mass transport. For vanadium RFB systems, IDFF and SFF are repeatedly reported to be the benchmark flow configuration. This is mostly due to both flow geometries naturally forcing the electrolyte to enter the electrode plane convectively and hence helps in improving the mass transport of the active species (Dennison *et al.* 2016). Inherent similarities between the utilized flow cells and the flow field geometries are expected to enhance the ion delivery to the electrode surfaces and pores. These modifications in ion delivery are anticipated to enhance the salt adsorption performance of the CDI system, same as in RFB's. The influence of ion delivery to the electrodes is investigated via testing IDFF, SFF, and PFF designs, coupled with five different flow rates (2, 8, 32, 64, and 128 mL/min).

Effect of flow rate on CDI performance

The ion concentration vs time plots for the CDI setup having IDFF and SFF are shown in Figure 3(a) and 3(b). Increasing flow rates are observed to negatively affect the salt removal performance of a CDI setup with IDFF or SFF. The SAC declines up to 51% and 49% are seen in CDI setups with IDFF or SFF, respectively. The loss of SAC with increasing flow rate for these setups is attributed to the underutilization of the electrodes due to the kinetic limitations introduced to the system via the decreasing residence time of saline water (Mossad & Zou 2012; Kim & Yoon 2015; Agartan *et al.* 2018). SFF shows negligible variations in the rate of concentration change with time as flow rate increases. On the other hand, IDFF shows more profound variations in the rate of change

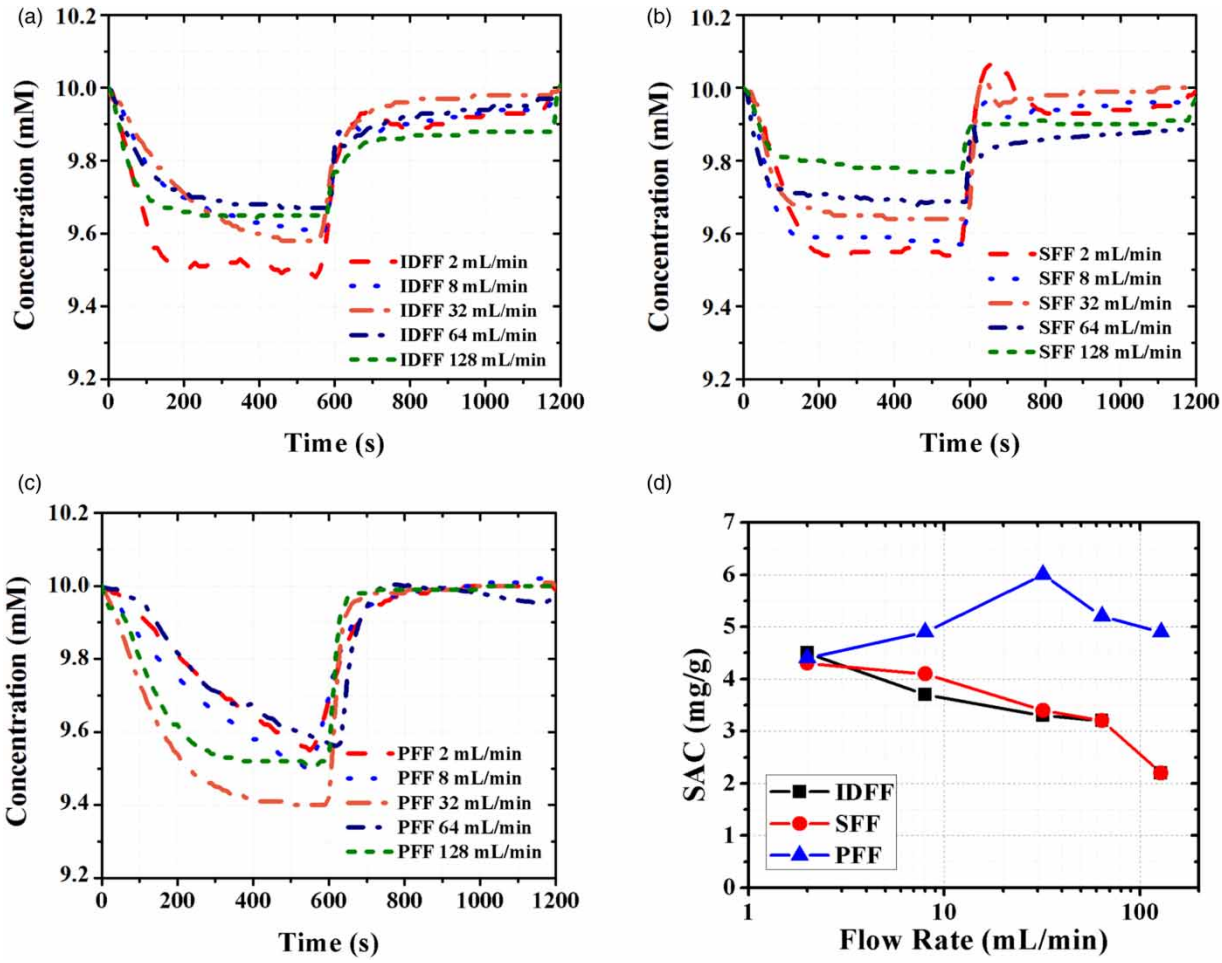

Figure 3 | Concentration vs time plots for (a) IDFF, (b) SFF, (c) PFF, and (d) SAC vs flow rate plot.

of concentration with time with increasing flow rate. Figure 3(c) shows the ion concentration vs time plots of the CDI setups having PFF. Unlike IDFF or SFF, PFF shows a parabolic (concave downwards) trend with an increasing flow rate. Although the flow rate and the residence time are inversely proportional to each other, SAC values show a remarkable increase (~37%) for the PFF_32 relative to PFF_2. Yet, the SAC slightly decreases when higher flow rates are applied. Although residence time is significantly less for the PFF_128 case as compared to the PFF_2 case, it removes ~12% more ions than the PFF_2 case, suggesting improved salt removal kinetics and enhanced ion delivery to the electrodes for the PFF_128 case. These observations suggest a strong dependence of the salt adsorption performance on the flow directionality of water in the flow channel.

The flow rate dependence of the SAC for each FF design is plotted in Figure 3(d). Unlike in a flow battery system, increasing flow rate is observed to cause significant performance loss for both the IDFF and the SFF designs in a CDI setup. On the other hand, PFF being the worst performing flow field design for the RFB systems (Dennison *et al.* 2016), outperforms both designs when integrated into a CDI setup. We believe that this discrepancy results from the differences between the charge storage mechanisms of two systems: faradaic (RFB) vs capacitive (CDI). This unusual trend observed between the applied flow rates and the SAC values for the PFF design highlights how differently the flow configuration can affect the salt removal performance for the capacitive electrodes. To further understand the effects of FF designs on the salt removal performance of a CDI system, 2 and 32 mL/min flow rates for all flow fields are investigated in more detail.

Effect of flow field design on CDI performance

In Figure 4(a), the ion concentration vs time graph for all FFs is given for 2 mL/min, SAC and charge efficiency values are listed in Table 1. Neither the SAC nor the charge efficiency values suggest any noteworthy influence of the employed flow field on the salt removal performance of a CDI system at 2 mL/min flow rate. Yet, the trend observed for the rate of changes in concentration with time for each flow field suggested influence of flow fields on the SAR of the CDI system. Due to the fact that the desalination performances of each flow field were compared for 32 mL/min flow rate to amplify the characteristic effects of them. In Figure 4(b), the ion concentration vs time plots for all flow fields are given for 32 mL/min, SAC and charge efficiency values are listed in Table 1. Both the SAC and charge efficiency results of the PFF_32 case diverge from the other configurations by showing notably improved performance. This is mostly attributed to the non-convective entrance of the saline water to the electrode plane in the case of open-ended channels (i.e., PFF) allowing a low-pressure flow. More profound influences of the employed flow field designs on desalination performances

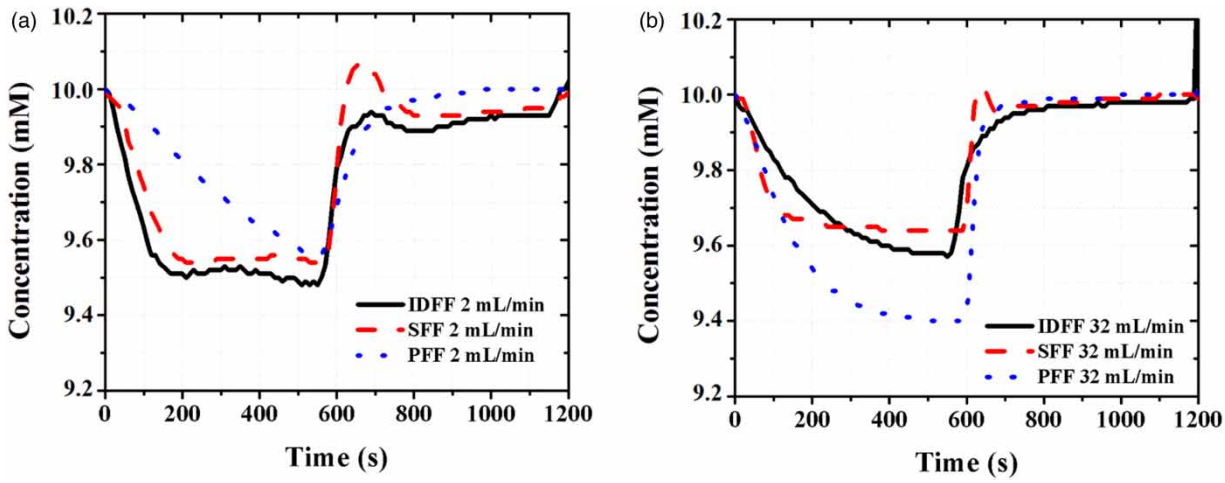

Figure 4 | Concentration vs time plots for all FF designs at (a) 2 and (b) 32 mL/min flow rates.

Table 1 | SAC and charge efficiency values for different flow field designs at 2 and 32 mL/min flow rates

Flow configuration	SAC (mg/g)	Charge efficiency (%)
IDFF_2	4.53	36.83
SFF_2	4.27	36.70
PFF_2	4.40	33.46
IDFF_32	3.31	29.66
SFF_32	3.41	29.44
PFF_32	6.02	41.90

of the electrodes are recorded with the application of faster flow rates, as Table 1 suggests.

Although the SAC and charge efficiency values for 2 mL/min cases are similar, the shapes and slopes of the recorded ion concentration data suggest differences between the electrosorption kinetics of the tested flow field designs (see Figure 4(a)). The IDFF_2 and the SFF_2 cases are observed to have reached saturation around the 3rd minute of charging, while the PFF_2 case has reached a similar ion concentration by the end of the 10th minute of charging. This observation suggests that electrosorption kinetics of the IDFF_2 and the SFF_2 cases are remarkably faster than the PFF_2 case due to the forced entry of the saline water to the electrode plane. On the other hand, the ion concentration vs time graphs for 32 mL/min (see Figure 4(b)) differ from the ones seen in Figure 4(a). The slope of the ion concentration vs time graph of the IDFF_32 is more horizontal than that of the IDFF_2, suggesting slower adsorption of ions at a higher flow rate. In the meantime, SFF design does not indicate any significant change in SAR with increasing the flow rate. On the other hand, the slope of the ion concentration vs time curve gets more vertical for the PFF_32 relative to PFF_2, suggesting faster ion adsorption at a higher flow rate. To better quantify this observation, the correlations between the electrosorption kinetics and flow configurations are investigated with the help of *in situ* SAR vs SAC plots.

Figure 5(a) shows the *in situ* SAR vs SAC plots for all flow fields at 2 mL/min. The initial sharp rise of SAR at IDFF_2 is followed by a plateau region until the electrode saturation. A rapid decline of SAR is recorded after saturation. The SAR of SFF_2 started with an increasing trend with SAC and have not plateaued. A gradual decline is observed, upon reaching the peak SAR value. In the meantime, the PFF_2 shows the lowest SAR among the tested flow fields. However, the SAR values calculated for PFF_2 are very steady throughout the whole charging period. The presence of a plateau region suggests salt removal occurring at a constant kinetic rate during charging and could offer steady-state salt removal operation enabling constant effluent concentration. Our results show that although SAC and charge efficiency values at 2 mL/min are similar for all the flow field designs, electrosorption kinetics is found to differ greatly depending on the type of flow induced in the cell. These results suggest that ion transportation is significantly affected by the flow directionality and varies significantly between different flow fields. Additionally,

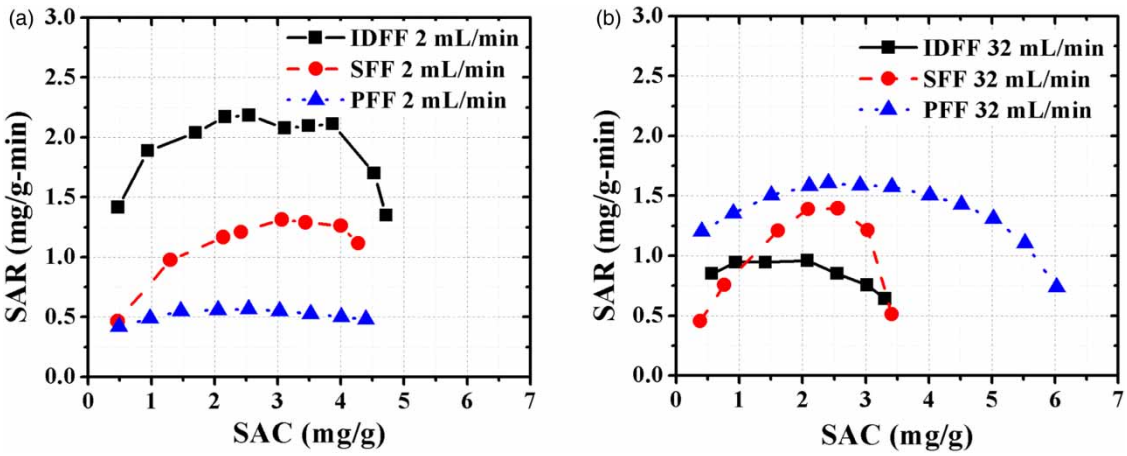

Figure 5 | *In situ* SAR vs SAC plot of different flow field designs at (a) 2 and (b) 32 mL/min flow rates.

extra insights provided by the *in situ* SAR vs SAC plots revealed the capabilities of *in situ* analyses for developing a better understanding of the salt removal behavior of a CDI system.

In Figure 5(b), *in situ* SAR vs SAC plots for all studied flow field designs at 32 mL/min are given. Variations in the salt removal performances at this increased flow rate are unique for each flow design. The IDFF_32 shows lower SAR accompanied by a notably decreased SAC (i.e., ~27%) relative to those of the IDFF_2. On the other hand, the SAR of the SFF_32 does not show any major change as compared to the SFF_2. However, the SFF_32 case has adsorbed 20% fewer ions than the SFF_2. On the contrary, the PFF_32 has adsorbed 37% more ions with notably increased SAR compared to PFF_2. Although SAC and charge efficiency values have shown no dependence on the flow field design for slow flow rates, as the flow rate increases, the effects of flow directionality have been observed to become more profound.

The different trends observed for each flow field design with increasing flow rates are attributed to the different interaction of flowing water with EDL, being dictated by the employed flow configuration. EDL theory suggests two layers within the charged layer. The attractive forces in the compact layer are strong enough to keep the ions immobile, as long as a potential difference is applied to the electrodes. However, the attractive forces acting on the ions held in the diffuse layer are much weaker (You & Guo 2010). In other words, if the hydrodynamic forces induced on the electrode surface can overcome the attractive forces between the ions and the electrode surface, ions can be ripped off from the diffuse layer causing significant loss to the SAC and deterioration to the kinetics.

The IDFF and SFF designs (see Figure 2(a) and 2(b)) force the water to move in the z-direction (toward the electrode plane), resulting in the movement of saline water and the electrostatic attractive forces (between the ions and the electrodes) to align in the same direction (z-direction; see Figure 2(a) and 2(b)). This alignment enables faster electrosorption kinetics at slower flow rates (2 mL/min). However, at higher flow rates, the hydrodynamic and convective forces increase and start ripping off ions from the diffuse layer in the cases of IDFF and SFF designs. Contrary to other flow fields, increasing the flow rate to 32 mL/min has increased the SAC (~37%) and the charge efficiency (~25%) of the PFF design. This unexpected performance enhancement is attributed to forcing water to rise toward the electrodes at higher flow rates. In the case of PFF design, the flow plane of water (xy-plane) inside the cell, and the electrostatic attractive forces (z-direction) are perpendicular to each other. This means ion transport toward the electrode surface is mostly dominated by the electrostatic forces, allowing much compact EDLs to form. Furthermore, increasing flow rate shows an improvement until moderate flow rates (i.e., 32 mL/min), indicating that if the drag forces induced by the increasing flow rate can be quickly compensated by the geometry of the flow field just as in PFF design, improvements in the salt removal performance can still be achieved at higher flow rates for capacitive systems.

Pressure drop and energy consumption analyses

The results discussed in the previous sections have shown a strong dependency of the salt removal performance on the selected flow configuration. Together with electrochemical efficiency, understanding the impact of the flow configuration on the hydraulic efficiency of the CDI systems is crucial to design a robust CDI system. To better understand the influence of flow directionality on the hydraulic losses and energy consumption of the CDI systems, two flow field designs having close-ended (i.e., IDFF) and open-ended (i.e., PFF) flow channels have been further studied.

In Figure 6(a), pressure drop vs flow rate plots for the IDFF and the PFF designs are given. Although the pressure drop increases with increasing flow rate for both flow field designs, IDFF shows a much higher (approximately sevenfold) pressure drop than PFF. This is expected due to the close-ended architecture of the flow channels in the IDFF design. The pressure drop values are very small for PFF that they are below the detection limit (0.05 psi = 0.34 kPa) of the employed pressure gauge until the 64 mL/min flow rate. The gap between the recorded pressure drop values for the IDFF and the PFF suggests that employed FF profoundly affects the flow directionality of the water inside the CDI cell as it has affected the salt removal performance. Increasing pressure drop is seen to have deteriorated the salt

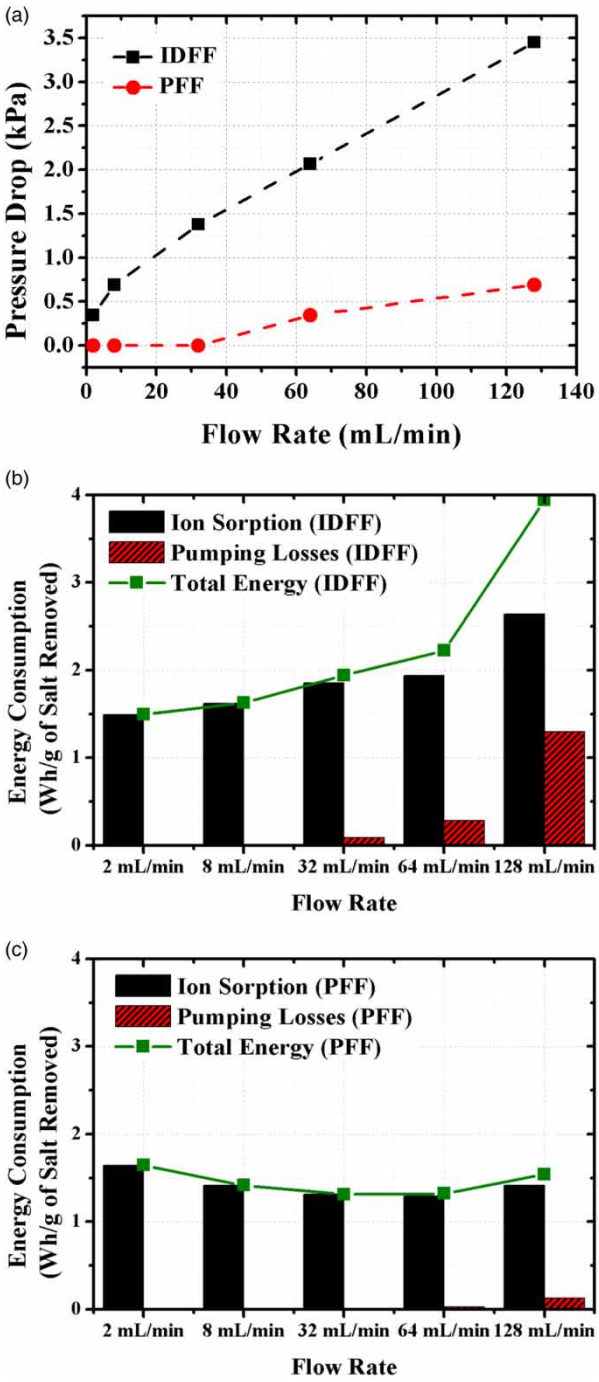

Figure 6 | (a) Pressure drop vs flow rate plots for IDFF and PFF, energy consumption vs flow rate plots for (b) IDFF, and (c) PFF.

removal performance of the CDI systems via disturbing the diffuse layer of the EDL.

The effects of the flow configuration on the energy consumption of the CDI systems are investigated for the IDFF and the PFF designs. Energy consumed for charging the electrodes and for pumping the water is considered in the calculation of the total energy consumption and normalized to the total mass of salt removed from the solution. In Figure 6(b), the energy consumption values for the IDFF cases are given. Increasing flow rate is observed to have significantly increased the energy consumed for both charging the electrodes and pumping the water (~167% increase from the IDFF_2 to the IDFF_128 case). The energy needed for charging the electrodes increases with flow rate due to decreased SAC values resulting from underutilization of the electrodes. As mentioned before, this underutilization is due to the ion rip-off from the diffuse layer of EDL as a result of dramatically increased pressure drop values. Furthermore, higher flow rates increased the required pumping energy as a result of escalated pressure drop values. Although the energy needed for charging the electrodes is higher than the energy needed for pumping the water at all flow rates, the change in pumping energy with the flow rate was found to be higher than the change in energy for charging with the IDFF.

In Figure 6(c), the energy consumption values for the PFF cases are given, and a remarkably different trend is observed with an increasing flow rate. In PFF design, increasing the flow rate leads to a parabolic (concave upwards) trend for energy consumption. The energy required for both charging and pumping have decreased with increasing flow rate until 32 mL/min. The PFF_32 is found to have consumed ~23% and ~38% less energy than those of PFF_2 and IDFF_32, respectively. Although energy consumption starts to increase after the 32 mL/min flow rate, the total energy needed for the PFF_128 is found to be ~6% smaller than that of the PFF_2. Furthermore, energy consumed by PFF_128 is found to be less than half of the energy consumed by the IDFF_128. In addition to that, the lower pressure drop values do not lead to ion rip-off from the diffuse layer, letting ion sorption energy consumption to stay steady and preventing the pumping energy to increase as much as it does for IDFF, as flow rate increases. The results obtained for the energy consumption analyses confirm the impact of the flow configuration on the performance metrics of the CDI system and suggest that if increased pumping pressure due to higher flow rates can be compensated by an improvement in the salt removal

performance, lower energy consumption metrics are still achievable.

CONCLUSION

Our systematic study of the impact of various flow configurations on the CDI performance of capacitive electrodes shows that mass transport considerations in cell design for CDI systems differ notably from faradaic systems (i.e., RFBs). Salt removal performance is found to depend strongly on the employed flow field, indicating that the directionality of flow inside the CDI cell could profoundly affect the formation of the EDL and the resulting salt adsorption performance. For instance, CDI cells containing IDFF or SFF designs are found to show a decreasing salt removal performance (~25% in SAC) with increasing flow rate due to the presence of excessive hydrodynamic forces when entering the electrode plane at high flow rates. On the other hand, for the parallel flow fields, the salt removal performance is found to peak around 32 mL/min (~37% increase). This suggests that an increase in the flow rate and the resulting hydrodynamic pressure could be compensated by the open-ended channels of the PFF design up to a point where effective delivery of the ions to the electrode surface could be achieved even at higher flow rates (32 mL/min).

Overall, the directionality of the flow induced in the CDI cells by different flow configurations is found to greatly impact the salt removal performance of the capacitive (ACC) electrodes. High-pressure inducing flow field designs (i.e., SFF and IDFF) are found to negatively impact the CDI performance due to convective flow of the saline water into the electrode plane, weakening the extent of EDL formation. On the other hand, flow field designs that can release the hydrodynamic pressures generated by the increased flow rate (e.g., PFF) is able to offer improved ion transport to the electrode surface even at higher flow rates without negatively affecting the EDL formation. Our findings provide new insights into the design of much effective and robust CDI cell architectures for capacitive electrodes, where high salt removal performances can be achieved with minimal losses in hydraulic efficiency to offer competitive desalination performance.

ACKNOWLEDGEMENTS

The authors would like to thank the National Science Foundation (Grant #1351161) for supporting this work.

REFERENCES

Agartan, L., Akuzum, B., Mathis, T., Ergenekon, K., Agar, E. & Kumbur, E. C. 2018 Influence of thermal treatment conditions on capacitive deionization performance and charge efficiency of carbon electrodes. *Separation and Purification Technology* **202**, 67–75.

Agartan, L., Hayes-Oberst, B., Byles, B., Akuzum, B., Pomerantseva, E. & Kumbur, E. C. 2019 Influence of operating conditions and cathode parameters on desalination performance of hybrid CDI systems. *Desalination* **452**, 1–8.

Aldalbahi, A., Rahaman, M., Almoiqli, M., Hamedelniel, A. & Alrehaili, A. 2018 Single-walled carbon nanotube (SWCNT) loaded porous reticulated vitreous carbon (RVC) electrodes used in a capacitive deionization (CDI) cell for effective desalination. *Nanomaterials (Basel)* **8**. doi:10.3390/nano8070527.

Biesheuvel, P. M. & van der Wal, A. 2010 Membrane capacitive deionization. *Journal of Membrane Science* **346**, 256–262.

Dennison, C. R., Agar, E., Akuzum, B. & Kumbur, E. C. 2016 Enhancing mass transport in redox flow batteries by tailoring flow field and electrode design. *Journal of Electrochemical Society* **163**, A5163–A5A69.

Gabelich, G. J., Tran, T. D. & Suffet, I. H. 2002 Electrosorption of inorganic salts from aqueous solution using carbon aerogels. *Environmental Science & Technology* **36**, 3010–3019.

Gao, X., Omosebi, A., Landon, J. & Liu, K. 2015 Surface charge enhanced carbon electrodes for stable and efficient capacitive deionization using inverted adsorption–desorption behavior. *Energy & Environmental Science* **8**, 897–909.

Han, L., Karthikeyan, K. G., Anderson, M. A. & Gregory, K. B. 2014 Exploring the impact of pore size distribution on the performance of carbon electrodes for capacitive deionization. *Journal of Colloid and Interface Science* **430**, 93–99.

Houser, J., Pezeshki, A., Clement, J. T., Aaron, D. & Mench, M. M. 2017 Architecture for improved mass transport and system performance in redox flow batteries. *Journal of Power Sources* **351**, 96–105.

Huang, W., Zhang, Y., Bao, S., Cruz, R. & Song, S. 2014 Desalination by capacitive deionization process using nitric acid-modified activated carbon as the electrodes. *Desalination* **340**, 67–72.

Jeon, S.-I., Park, H.-R., Yeo, J.-G., Yang, S. C., Cho, C. H., Han, M. H. & Kim, D. K. 2013 Desalination via a new membrane capacitive deionization process utilizing flow-electrodes. *Energy & Environmental Science* **6**, 1471.

Kim, T. & Yoon, J. 2015 CDI ragone plot as a functional tool to evaluate desalination performance in capacitive deionization. *RSC Advances* **5**, 1456–1461.

Laxman, K., Myint, M. T. Z., Khan, R., Pervez, T. & Dutta, J. 2015 Improved desalination by zinc oxide nanorod induced electric field enhancement in capacitive deionization of brackish water. *Desalination* **359**, 64–70.

Lee, J. Y., Seo, S. J., Yun, S. H. & Moon, S. H. 2011 Preparation of ion exchanger layered electrodes for advanced membrane capacitive deionization (MCDI). *Water Research* **45**, 5375–5380.

Lee, J., Kim, S., Kim, C. & Yoon, J. 2014 Hybrid capacitive deionization to enhance the desalination performance of capacitive techniques. *Energy & Environmental Science* **7**, 3683–3689.

Mossad, M. & Zou, L. 2012 A study of the capacitive deionisation performance under various operational conditions. *Journal of Hazardous Materials* **213–214**, 491–497.

Omosebi, A., Gao, X., Rentschler, J., Landon, J. & Liu, K. 2015 Continuous operation of membrane capacitive deionization cells assembled with dissimilar potential of zero charge electrode pairs. *Journal of Colloid and Interface Science* **446**, 345–351.

Porada, S., Zhao, R., van der Wal, A., Presser, V. & Biesheuvel, P. M. 2013 Review on the science and technology of water desalination by capacitive deionization. *Progress in Materials Science* **58**, 1388–1442.

Ratajczak, P., Suss, M. E., Kaasik, F. & Béguin, F. 2019 Carbon electrodes for capacitive technologies. *Energy Storage Materials* **16**, 126–145.

Remillard, E. M., Shocron, A. N., Rahill, J., Suss, M. E. & Vecitis, C. D. 2018 A direct comparison of flow-by and flow-through capacitive deionization. *Desalination* **444**, 169–177.

Ryoo, M.-W., Kim, J.-H. & Seo, G. 2003 Role of titania incorporated on activated carbon cloth for capacitive deionization of NaCl solution. *Journal of Colloid and Interface Science* **264**, 414–419.

Srimuk, P., Kaasik, F., Krüner, B., Tolosa, A., Fleischmann, S., Jäckel, N., Tekeli, M. C., Aslan, M., Suss, M. E. & Presser, V. 2016 MXene as a novel intercalation-type pseudocapacitive cathode and anode for capacitive deionization. *Journal of Materials Chemistry A* **4**, 18265–18271.

Suss, M. E., Porada, S., Sun, X., Biesheuvel, P. M., Yoon, J. & Presser, V. 2015 Water desalination via capacitive deionization: what is it and what can we expect from it? *Energy & Environmental Science* **8**, 2296–2319.

Wang, J. 2015 Theory and practice of flow field designs for fuel cell scaling-up: a critical review. *Applied Energy* **157**, 640–663.

Yang, J., Zou, L., Song, H. & Hao, Z. 2011 Development of novel MnO_2/nanoporous carbon composite electrodes in capacitive deionization technology. *Desalination* **276**, 199–206.

You, X.-Y. & Guo, L. 2010 Combined effects of EDL and boundary slip on mean flow and its stability in microchannels. *Comptes Rendus Mécanique* **338**, 181–190.

First received 27 January 2019; accepted in revised form 17 January 2020. Available online 13 February 2020